Digumarti, K. M., Cao, C., Guo, J., Conn, A. T., & Rossiter, J. (2018). Multi-directional crawling robot with soft actuators and electroadhesive grippers. In *2018 IEEE International Conference on Soft Robotics (RoboSoft 2018): Proceedings of a meeting held 24-28 April 2018, Livorno, Italy* (pp. 303-308). Institute of Electrical and Electronics Engineers (IEEE). https://doi.org/10.1109/ROBOSOFT.2018.8404936

Multi-directional Crawling Robot with Soft Actuators and Electroadhesive Grippers

Krishna Manaswi Digumarti[1,†], Chongjing Cao[1,†], Jianglong Guo[1,3], Andrew T. Conn[1,2] and Jonathan Rossiter[1,3]

***Abstract*— This paper presents the design of a planar, low profile, multi-directional soft crawling robot. The robot combines soft electroactive polymer actuators with compliant electroadhesive feet. A theoretical model of a multi-sector dielectric elastomer actuator is presented. The relation between actuator stroke and blocking force is experimentally validated. Electrostatic adhesion is employed to provide traction between the feet of the robot and the crawling surface. Shear force is experimentally determined and forces up to 3N have been achieved with the current pad design. A 2D multi-directional gait is demonstrated with the robot prototype. Speeds up to 12mm/s (0.1 body-lengths/s) have been observed. The robot has the potential to move on a variety of surfaces and across gradients, a useful ability in scenarios involving exploration.**

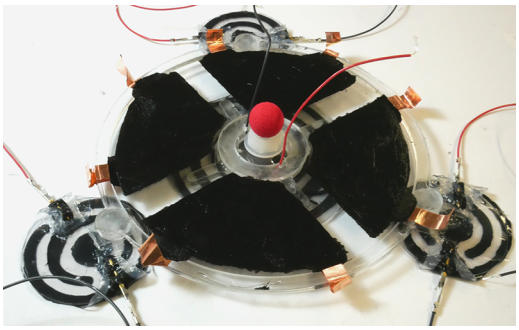

Fig. 1. A prototype of the proposed crawling robot.

I. INTRODUCTION

Locomotion is a key requirement in a robot designed for exploration. The ability to move without being hindered by undulations in terrain or steep gradients is particularly useful. Some robots overcome these challenges by using articulated legs. While these are largely successful [1],[2], they are not suitable where space is a constraint. Robots that move closer to the ground in a manner similar to crawling are more suited to such a scenario [3-6,11-13]. This paper presents the design of a novel low profile crawling robot that has the potential to move on a variety of surfaces and across any gradient.

Different approaches have been presented in the literature on the design crawling robots, exploiting softness to varying degrees. Worm-like robots such as the SoftWorm[3] and the CMMWorm[4] rely on mechanical actuation and require large complex structures to accommodate large actuators. On the other hand, the Meshworm[5], which uses coiled shape memory alloy actuators is completely soft and flexible. However, these actuators have a slow actuation-relaxation cycles limited by thermodynamic constraints. Pneumatic actuation has also been used to achieve crawling by employing purpose designed networks of chambers [6], [7]. These robots either require large actuation systems external to the robot or exhibit slow locomotion owing to limitation in the rate of actuation of on-board systems.

In recent times, the use of electro-active polymers, particularly dielectric elastomer actuators (DEA), has become popular in the design of soft crawling robots. These soft and inherently compliant actuators have certain advantages over conventional actuators. They exhibit large active strains, high energy density, are scalable and can be manufactured at a low cost [8]. They have been used in different configurations to achieve locomotion. A cylindrical hydrostatic push-pull actuator made of DEA is presented in [9]. A unidirectionally expanding DEA structure is used in [10] to replicate an inchworm like locomotion. Stacks of actuators are employed in [11] to realize an annelid locomotion and are also used in [12] to present a four limbed crawler. A minimum energy structure is used in [13] to design another inchworm type robot. Cone shaped actuators with multiple degrees of freedom have also been used in a hexapod [14]. Most of these robots move in a single direction, restricted by the configuration of the actuators. In this paper, a planar multi-sector disk shaped DEA configuration is used, which provides actuation in two orthogonal directions, enabling the robot to move in any direction on a plane. We first present a theoretical model to predict the blocking force at different stroke lengths. This model is experimentally validated and the actuator is used in a crawling robot.

In addition to having an actuation system, anisotropic friction is required to generate forward motion. Many methods to achieve this asymmetry have been explored in the context of crawling robots. These range from simple bristles [9] and pins [10],[12] to bio-inspired adhesives [15]. A common limitation of these methods is that the motion is restricted to one direction and is affected by surface properties such as roughness. In this work, we take an approach similar to that of [13] and make use of electrostatic adhesion (EA) to achieve frictional anisotropy. EA is easy to control and provides the ability to adhere to multiple surface types, both

[1]Bristol Robotics Laboratory, University of Bristol and University of the West of England, BS16 1QY, UK

[2]Department of Mechanical Engineering, University of Bristol, BS8 1TR, UK

[3]Department of Engineering Mathematics, University of Bristol, BS8 1UB, UK

† KMD and CC contributed equally (and are joint first authors) km.digumarti@bristol.ac.uk, cc15716@bristol.ac.uk

Video: https://youtu.be/nEBLiJr5is4

electrically conductive and insulating [16]. Friction can be introduced on demand in any direction, which greatly expands the orientations and environments that can be operated in. Particularly in the case of an autonomous soft robot using DEA, it has the added benefit of using electric potential to drive both the robot and provide traction.

In this paper, a multi-sector disk DEA is used in combination with EA feet to design a crawling robot. A prototype of the robot is shown in fig. 1. First, a theoretical model of the multi-sector DEA is presented. Following this, the process of fabrication is presented. Experiments to validate the relationship between blocking force and stroke of the DEA are carried out. The working of the EA pads on different material surfaces is shown. The design of the crawling robot is then presented along with an analysis of its walking pattern and results from tests on its locomotion.

II. Multi-sector disk DEA

A. Design overview and actuation principle

The multi-sector disk DEA is a planar simplification of [17],[18]. It consists of a DEA membrane bonded to a rigid ring frame and a smaller central disk, while the region in between is free to move. This free area is then divided into four sectors, each of which can be actuated separately. When voltage is applied across the electrodes of one sector, the expansion in area of this sector moves the central disk relative to the frame. The actuation of different sectors results in a two degrees-of-freedom (DoF) movement, as illustrated in fig. 2.

Fig. 2. Actuation principle of the four sector disk DEA. Red shows the actuated segment and consequent movements of the rigid central disk.

B. DEA model

A simplified model is proposed in this work to quantify the stroke and blocking force relationship of the disk DEA. The approach is similar to that in [19]. Due to the symmetry of this DEA design, we only analyze the actuation in one direction. Simplifying assumptions are made in this model, which include:

i the circumferential deformation does not contribute to the stroke and force output;
ii the circumferential stretch ratio is constant and is not affected by the actuation;
iii the elastomer is incompressible.

A circular coordinate system is used, where the pole is the centre of the central disk, while the polar axis coincides with the symmetry axis of the actuated sector, as depicted in fig. 3.

Let region ($[r_{in} r_{out}]$, $[-\theta_A \theta_A]$) be the actuated sector and an electric field $E = V/T$ be applied across the electrodes of this section, where r_{in} is the radius of the inner disk and

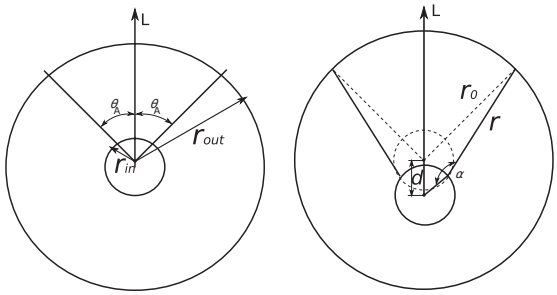

Fig. 3. Illustration of the actuation principle in terms of circular coordinates. r_{in} is the radius of the inner rigid disk and r_{out} is the inner radius of the outer ring. d is the displacement of the central disk. (a) shows unactuated and (b) shows a segment actuated.

r_{out} is the inner radius of the outer ring, θ_A is the angular coordinate of the boundary of the active region, V is the voltage and T is the thickness of the membrane. Let $r_0 = r_{out} - r_{in}$ be the initial radius of the DEA. Assuming the central disk moves a distance d relative to the outer ring, then the radius at angle θ becomes

$$r(\theta) = \sqrt{r_0^2 + d^2 - 2r_0 d\cos(\pi - \theta)}. \tag{1}$$

The Gent nonlinear materials model [20] is adopted to characterize the radial stress

$$\sigma_1 = \frac{\mu(\lambda_1^2 - \lambda_1^{-2}\lambda_2^{-2})}{1 - (\lambda_1^2 + \lambda_2^2 + \lambda_1^{-2}\lambda_2^{-2} - 3)/J} - \epsilon_0\epsilon_r E^2, \tag{2}$$

where $\lambda_1 = \lambda_{1pre} r/r_0$ is the radial stretch ratio, $\lambda 2 = \lambda_{2pre}$ is the circumferential stretch ratio, λ_{1pre} and λ_{2pre} are the radial and circumferential pre-stretch ratios respectively, ϵ_0 and ϵ_r are the absolute and relative dielectric permittivity respectively, μ is the shear modulus and J is the material constant related to the limiting stretch. In this study, μ = 30kPa and J = 150N/m^2 are used. These parameters are selected to achieve the best fit to the experimental data, and are in the range recommended in [21], [22] and [23].

The radial force of an infinitesimal section at angular coordinate θ can be expressed as

$$dF(\theta, E) = \sigma_1(\theta, E)^\top r(\theta)\, d\theta, \tag{3}$$

so the force output, which is the overall force on the central disk on the polar axis is an integration of $dF(\theta)$, and is given as

$$\begin{aligned} F = &\int_{-\theta_A}^{\theta_A} dF(\theta, E = E_0)\cos(\alpha)\cos(\theta) \\ &+ \int_{\theta_A}^{2\pi-\theta_A} dF(\theta, E = 0)\cos(\alpha)\cos(\theta) \end{aligned} \tag{4}$$

where

$$\cos(\alpha) = \frac{r_0^2 + r^2 - d^2}{2rr_0} \tag{5}$$

III. Electrostatic Adhesion

A simplified model [24] can be used to describe the EA force between two contacting surfaces in the presence of an electric field. Consider an EA pad of area A, the electrodes of which are at a potential difference V. If this pad is in contact with a surface, the force of attraction F_N can be given as

$$F_N = \frac{1}{8}\epsilon_0\epsilon_r A\frac{V^2}{d^2}, \tag{6}$$

where d is the thickness of the dielectric medium between the electrodes and the surface. This force acts normal to the surface. The critical shear force, F_S, defined as the peak force acting along the surface, at which the pad separates from the surface can then be given in terms of the coefficient of friction μ_f as

$$F_S = \mu_f F_N. \tag{7}$$

This shows a quadratic relation between applied voltage and the critical shear force. However, in practice it has been found that several parameters influence this force. A summary of these parameters is discussed in [25]. The problem is compounded if multiple electrode pairs are used to generate adhesion such as in the case of interdigitated electrodes. Theoretical and simulation models have been proposed but as reported in [26], there is inconsistency in predicting the force of attraction. Therefore, in this work, an experimental approach is taken.

IV. Fabrication

A. Fabrication of DEA

The dielectric elastomer actuator was fabricated from a single layer of VHB 4905 from 3M. The membrane was subject to equi-biaxial pre-stress of 4x4 and bonded to an acrylic ring frame of radius 50mm and an acrylic central disk of radius 15mm. This resulted in an elastomer membrane of 31.25μm thickness. Four electrodes were painted on each side of the membrane using carbon grease (MG chemicals). Each electrode pair covers one quarter of the membrane. Copper tape was used as a connection between the compliant electrodes and high voltage cables. A schematic representation is shown in fig. 7.

B. Fabrication of EA feet

A circular concentric ring pattern of electrodes was chosen for the design of the EA feet. See fig. 4 (f,g). This pattern produces a more symmetric force as opposed to a rectangular pattern [27]. This is desirable since the robot moves in multiple directions. The electrode tracks have a width of 3mm and a thickness of 0.1mm with a spacing of 4mm in between. Three pads of diameter 36mm were fixed to the body. One larger pad of diameter 60mm was fixed to the centre of the DEA membrane.

The electro-adhesive pads are fabricated by casting multiple layers of silicone in a manner similar to that presented in [24]. Instead of an engraved mould, a mask is used to form the electrode region. This enables quick changes in design if required. The order of constructing the layers is reversed as compared to the method in [24]. Ecoflex 00-30 from Smooth-On has been chosen as the elastomer material. First, a thin layer is deposited on an acrylic disk by spin coating. The disk is spun at a speed of 50rpm for 10s followed by a speed of 1000rpm for 60s. After this layer cures, the electrode layer is cast on top of it. Carbon black (Vulcan VXC72R, Cabot Corporation) was mixed with Ecoflex at a concentration of 5% by weight to make a conductive elastomer. A mask forming the pattern of electrodes was cut out on paper and placed on the cured first layer. The electrodes were then painted through the mask and any excess was scraped off. After curing, the electrodes were enclosed in a third insulating elastomer layer. See fig. 4 for a pictorial representation. A 0.02mm thin sheet of mylar was affixed to the bottom of the pad to reduce tackiness of the surface.

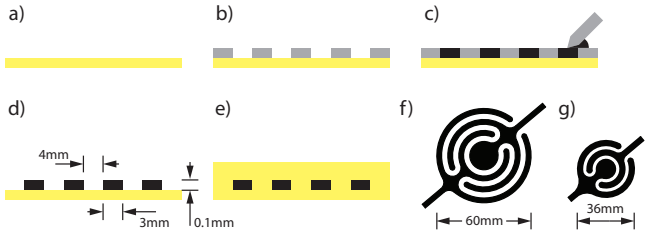

Fig. 4. Stages of fabrication of electro-adhesive pad. a) A thin layer of elastomer is spun coat on an acrylic surface. b) A paper mask is laid on top of the first layer after it cures. c) Conductive silicone is applied through the mask. d) The mask is peeled off and the second layer is allowed to cure. e) A final layer of elastomer is applied to enclose the electrodes. f) The pattern used for the central foot. g) The pattern used for the feet on the sides.

V. Experiments

A. DEA Blocking force

The first experiment was to measure the blocking force output of the DEA as a function of displacement, d. The DEA was fabricated as described in section IV-A. A load cell and the frame of the DEA were clamped to a rigid testing rig. The central disk of the actuator was attached to the load cell using a string. An electric field of $E_0 = 100V/\mu m$ was applied to the DEA which in turn pulled the string. The blocking force of the DEA was thus measured on the load cell. Measurements were taken for strokes in the range of 0 to 4mm. The experiment was repeated three times for each stroke to eliminate error. All experiments were performed in a temperature controlled room maintained at 20^{o}C. Figure 5 shows the comparison between the model prediction and experimental results. Both show that the blocking force and stroke relationship is approximately linear. This DEA design is able to exert a maximum force of 400mN at $E_0 = 100V/\mu m$ and a linear stroke of 4mm in the plane of actuation. A very good agreement can be seen between the predicted and experimental results in fig. 5.

B. EA shear force

Adhesion of the foot to different materials was tested by measuring the shear force between the EA pad and the

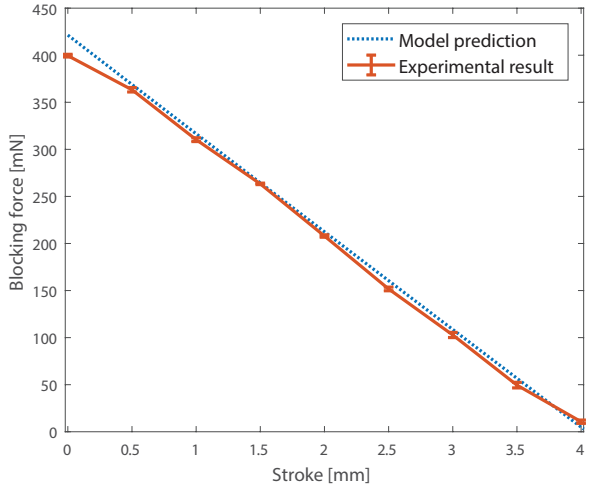

Fig. 5. Blocking force of a single DEA at different stroke lengths.

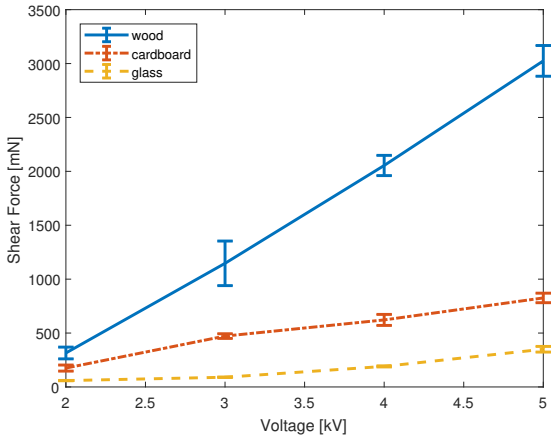

Fig. 6. Shear force due to EA as a function of charging voltage on different surfaces. The EA pad has a circular geometry with an outer diameter of 60mm.

test surface. The larger central pad of 60mm diameter was used for all experiments. Three different materials were used, namely finished wood, cardboard and glass. The experimental setup was as follows. The pad was placed on the test surface. A nylon ring was then affixed to the top surface of the pad. A load cell fixed to a moving platform was used to pull this ring while the pad was activated. First the pad was moved across the test surface without any activation voltage. The peak force measured in this case gives the static frictional force between the two surfaces. A voltage was then applied across the electrodes of the pad. The pad was held stationary for 10s to avoid the influence of time-related effects of the electric field. The pad was then moved and the force required to move the pad was measured. Subtracting the force due to static friction from this value gives the shear force due to EA. Force was measured for different actuation voltages in the range of 2kV to 5kV. Each trial was repeated five times. The critical shear force was recorded for each case, as shown in fig. 6.

It can be seen that the critical shear force follows a linear trend as activation voltage increases. This trend is similar to that presented in [13]. There is a larger deviation in force on wood, a nonuniform medium, as opposed to cardboard and glass, both more uniform media. In the case of glass, higher shear resistance has been reported in the literature [28] but these were obtained at higher activation voltages.

VI. Crawling Robot

A. Design

Based on the study of DEA blocking force and EA shear resistance presented above, a crawling robot has been designed. The main actuator is a four-sector DEA. The robot consists of one large central EA foot attached to the DEA membrane and three smaller EA feet attached to the frame. The smaller feet are attached to the outer edge of the frame at 120°angular spacing, as shown in fig. 1. The feet are adjusted in height such that the weight of the body is equally distributed between the central foot and the outer feet. This is achieved by using thin sheets of cellulose acetate. A schematic of different layers can be seen in fig. 7. A light red ball was fixed to top surface of the membrane in the centre to aid in tracking the position of the robot. The entire robot weighs 20g.

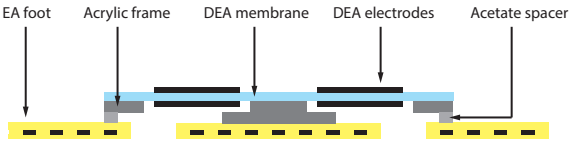

Fig. 7. A sectional view of the robot showing its different parts.

B. Concept of Locomotion

To achieve walking motion, actuation is provided in a specific pattern. The different stages of actuation are shown in fig. 8. They can be described as follows.

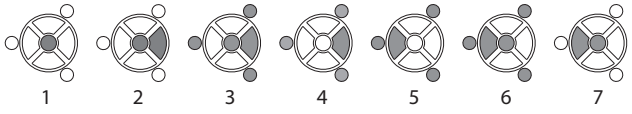

Fig. 8. Stages of actuation of the robot. Shaded regions indicate the DEA sector and EA foot that is active in each stage.

1: Activate the central EA foot.
2: Actuate the front DEA in the direction of motion. The body moves forwards as the central foot is holding its position.
3: Activate the EA feet on the sides. Front DEA is still actuated.
4: Deactivate the central EA foot. Front DEA is still actuated. The body holds its displaced position.
5: Actuate the rear DEA in the direction of actuation. Front DEA is simultaneously discharged. As a result, the central foot moves forwards.

6: Activate the central EA foot. It now holds the displaced position. Rear DEA is still actuated.
7: Deactivate the EA feet on the sides. Rear DEA is still actuated.
8: Rear DEA is discharged. The body moves forwards slightly. One cycle is complete and the robot is back to stage 1.

C. Control

To obtain the desired sequence of motion as described above, each actuator is controlled separately. The control structure is shown in fig. 9. Each DEA is independently energized and discharged by a pair of relays (K_i in fig. 9). These relays are opened and closed based on digital signals issued from a computer through an NI DAQ (USB-6343). The high voltage required to activate the DEA is provided by means of an amplifier (EMCO F121). A bleeding resistor of 4MΩ was used to safely discharge the DEA. In case of the EA feet, two separate high voltage channels are used, one for the central foot and the other for the three feet combined. These channels are provided from two independent high voltage amplifiers (UltraVolt 5HVA23-BPI).

A step function was used to charge and discharge each actuator. In case of the EA feet, it was found that a simple drop in applied voltage was not sufficient to make the pad release quickly from the surface it was in contact with. From practice, it was found that a decaying sinusoidal input enabled quicker release of the feet.

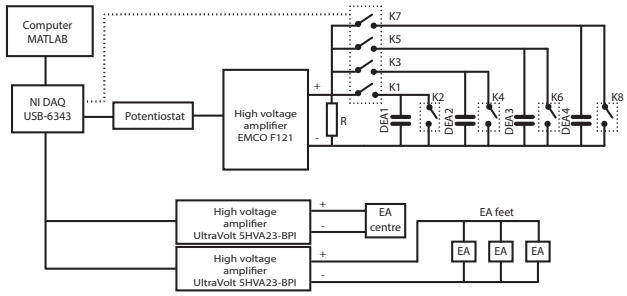

Fig. 9. Schematic diagram of the controller of the robot.

D. Locomotion tests

Shown in fig. 10 are a series of pictures of the robot when executing five steps of movement in one direction. The images are taken at the starting position, and after three and five cycles of movement. In this demonstration, a cycle takes 1.75s to complete. The voltage used for actuating DEA was 3.125kV, to activate the outer EA feet was 3kV each and for the inner EA foot was 4kV. Figure 11 shows the position of the robot in the plane as tracked by processing frames of video shot from above the robot. In this arbitrary trajectory, the robot takes three consecutive steps in one direction (t_0 to t_3), followed by three steps in a perpendicular direction (t_3 to t_6). The change in direction is achieved by activating the pair of actuators that are in line with the desired motion. This shows that the robot can successfully move in two perpendicular directions. In theory, the robot can move in any direction on the plane through appropriate control of all four actuators. Exploring this behaviour is left as a future task.

The speed of the robot can be controlled by changing the frequency of actuation. Figure 12 shows a plot of the speed of the robot as a function of actuation frequency. A trade off between stroke length and frequency affects the velocity at which the robot moves. At lower frequencies, the actuators exhibit longer strokes but the robot moves slower because the stroke occurs fewer times in a given period of time. At higher frequencies the stride rate is increased until the response is saturated by viscoelastic damping, which is a well known characteristic of VHB 4905. A maximum speed of 12mm/s was observed at an optimal frequency of 2.5Hz which equates to 0.1 body-lengths/s.

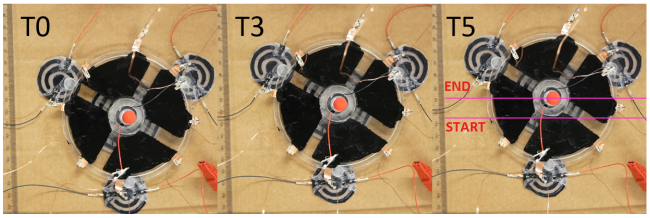

Fig. 10. The robot in its starting position (T0), after three steps of movement (T3) and after five steps of movement (T5). Refer to accompanying video.

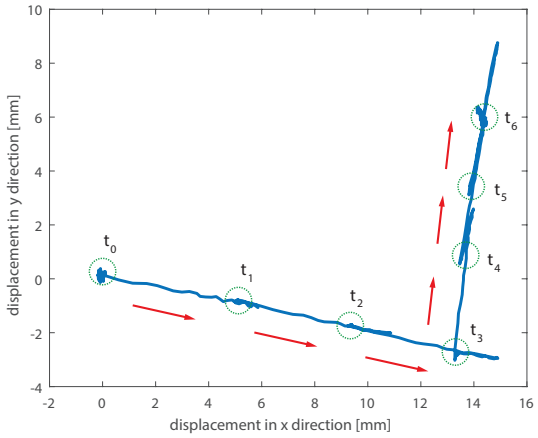

Fig. 11. Position of the robot tracked using image processing. The robot takes three steps in one direction followed by three more steps in the perpendicular direction, demonstrating its two degrees of movement.

VII. CONCLUSIONS

This paper has demonstrated a proof of concept for a planar multiple degrees of freedom crawling robot. We first presented a simplified model of a multi-sector dielectric elastomer actuator. The relationship between stroke and blocking force was experimentally verified. Critical shear force due to EA on different surfaces was experimentally determined. A maximum shear force of 3N was achieved on a wooden surface with the design presented here. The robot achieved

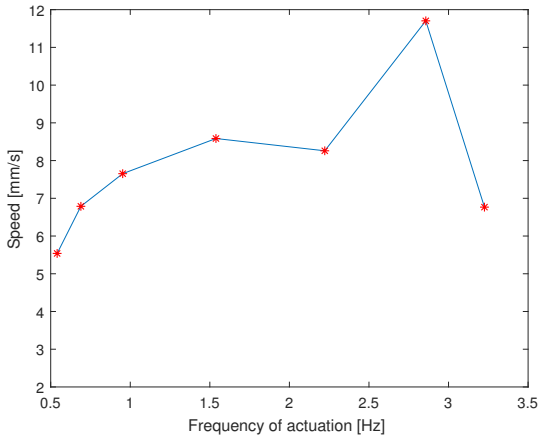

Fig. 12. Speed of the robot at different actuation frequencies. Optimum speed of 12mm/s is reached at 2.5Hz.

a maximum speed close to 12mm/s and demonstrated its ability to move in multiple directions.

In future work we plan to improve the robot in terms of its maximum speed and study its performance over uneven and non-horizontal surfaces. The effect of the size of the dielectric elastomer on velocity will also be investigated. Payload capacity of the robot is currently being studied. Changes in the material of construction are also being investigated.

ACKNOWLEDGMENT

This work was supported by the EPSRC centre for doctoral training in Future Autonomous and Robotic Systems (FARSCOPE) (EP/L015293/1) at the Bristol Robotics Laboratory where KMD and CC are PhD students, and EPSRC grants EP/P025846/1, EP/M020460/1 and EP/M026388/1.

REFERENCES

[1] C. Gehring, C. D. Bellicoso, S. Coros, M. Bloesch, P. Fankhauser, M. Hutter, and R. Siegwart, "Dynamic trotting on slopes for quadrupedal robots," in *Intelligent Robots and Systems (IROS), 2015 IEEE/RSJ International Conference on*, pp. 5129–5135, IEEE, 2015.

[2] M. Hutter, C. Gehring, D. Jud, A. Lauber, C. D. Bellicoso, V. Tsounis, J. Hwangbo, K. Bodie, P. Fankhauser, M. Bloesch, *et al.*, "Anymal-a highly mobile and dynamic quadrupedal robot," in *Intelligent Robots and Systems (IROS), 2016 IEEE/RSJ International Conference on*, pp. 38–44, IEEE, 2016.

[3] A. S. Boxerbaum *et al.*, "Continuous wave peristaltic motion in a robot," *The international journal of Robotics Research*, vol. 31, no. 3, pp. 302–318, 2012.

[4] A. D. Horchler, A. Kandhari, K. A. Daltorio, *et al.*, "Worm-like robotic locomotion with a compliant modular mesh," in *Conference on Biomimetic and Biohybrid Systems*, pp. 26–37, Springer, 2015.

[5] S. Seok, C. D. Onal, K.-J. Cho, *et al.*, "Meshworm: a peristaltic soft robot with antagonistic nickel titanium coil actuators," *IEEE/ASME Transactions on mechatronics*, vol. 18, no. 5, pp. 1485–1497, 2013.

[6] M. T. Tolley, R. F. Shepherd, B. Mosadegh, K. C. Galloway, M. Wehner, M. Karpelson, R. J. Wood, and G. M. Whitesides, "A resilient, untethered soft robot," *Soft Robotics*, vol. 1, no. 3, pp. 213–223, 2014.

[7] R. F. Shepherd, F. Ilievski, W. Choi, S. A. Morin, A. A. Stokes, A. D. Mazzeo, X. Chen, M. Wang, and G. M. Whitesides, "Multigait soft robot," *Proceedings of the National Academy of Sciences*, vol. 108, no. 51, pp. 20400–20403, 2011.

[8] F. Carpi, R. Kornbluh, P. Sommer-Larsen, and G. Alici, "Electroactive polymer actuators as artificial muscles: are they ready for bioinspired applications?," *Bioinspiration & biomimetics*, vol. 6, no. 4, p. 045006, 2011.

[9] A. T. Conn, A. D. Hinitt, and P. Wang, "Soft segmented inchworm robot with dielectric elastomer muscles," in *Electroactive Polymer Actuators and Devices (EAPAD) 2014*, vol. 9056, p. 90562L, International Society for Optics and Photonics, 2014.

[10] S. Shian, K. Bertoldi, and D. R. Clarke, "Use of aligned fibers to enhance the performance of dielectric elastomer inchworm robots," in *Proc. SPIE*, vol. 9430, pp. 94301–94309, 2015.

[11] K. Jung, J. C. Koo, Y. K. Lee, H. R. Choi, *et al.*, "Artificial annelid robot driven by soft actuators," *Bioinspiration & biomimetics*, vol. 2, no. 2, p. S42, 2007.

[12] M. Duduta, D. R. Clarke, and R. J. Wood, "A high speed soft robot based on dielectric elastomer actuators," in *Robotics and Automation (ICRA), 2017 IEEE International Conference on*, pp. 4346–4351, IEEE, 2017.

[13] J. Cao, L. Qin, H. P. Lee, and J. Zhu, "Development of a soft untethered robot using artificial muscle actuators," in *Electroactive Polymer Actuators and Devices (EAPAD) 2017*, vol. 10163, p. 101631X, International Society for Optics and Photonics, 2017.

[14] C. T. Nguyen, H. Phung, H. Jung, U. Kim, T. D. Nguyen, J. Park, H. Moon, J. C. Koo, and H. R. Choi, "Printable monolithic hexapod robot driven by soft actuator," in *Robotics and Automation (ICRA), 2015 IEEE International Conference on*, pp. 4484–4489, IEEE, 2015.

[15] D. Santos, B. Heyneman, S. Kim, N. Esparza, and M. R. Cutkosky, "Gecko-inspired climbing behaviors on vertical and overhanging surfaces," in *Robotics and Automation, 2008. ICRA 2008. IEEE International Conference on*, pp. 1125–1131, IEEE, 2008.

[16] D. Ruffatto, J. Shah, and M. Spenko, "Optimization and experimental validation of electrostatic adhesive geometry," in *Aerospace Conference, 2013 IEEE*, pp. 1–8, IEEE, 2013.

[17] H. Choi, K. M. Jung, J. Kwak, S. Lee, H. Kim, J. W. Jeon, and J. Nam, "Digital polymer motor for robotic applications," in *Robotics and Automation, 2003. Proceedings. ICRA'03. IEEE International Conference on*, vol. 2, pp. 1857–1862, IEEE, 2003.

[18] Y. Bar-Cohen, *Electroactive polymer (EAP) actuators as artificial muscles: reality, potential, and challenges*, vol. 136. SPIE press, 2004.

[19] P. Wang and A. T. Conn, "Elastic cube actuator with six degrees of freedom output," in *Actuators*, vol. 4, pp. 203–216, 2015.

[20] A. Gent, "A new constitutive relation for rubber," *Rubber chemistry and technology*, vol. 69, no. 1, pp. 59–61, 1996.

[21] Y. Wang, B. Chen, Y. Bai, H. Wang, and J. Zhou, "Actuating dielectric elastomers in pure shear deformation by elastomeric conductors," *Applied Physics Letters*, vol. 104, no. 6, p. 064101, 2014.

[22] C. Chiang Foo, S. Cai, S. Jin Adrian Koh, S. Bauer, and Z. Suo, "Model of dissipative dielectric elastomers," *Journal of Applied Physics*, vol. 111, no. 3, p. 034102, 2012.

[23] C. Zhang, H. Chen, L. Liu, and D. Li, "Modelling and characterization of inflated dielectric elastomer actuators with tubular configuration," *Journal of Physics D: Applied Physics*, vol. 48, no. 24, p. 245502, 2015.

[24] J. Germann, B. Schubert, and D. Floreano, "Stretchable electroadhesion for soft robots," in *Intelligent Robots and Systems (IROS 2014), 2014 IEEE/RSJ International Conference on*, pp. 3933–3938, Ieee, 2014.

[25] J. Guo, M. Tailor, T. Bamber, M. Chamberlain, L. Justham, and M. Jackson, "Investigation of relationship between interfacial electroadhesive force and surface texture," *Journal of Physics D: Applied Physics*, vol. 49, no. 3, p. 035303, 2015.

[26] J. Guo, T. Bamber, M. Chamberlain, L. Justham, and M. Jackson, "Optimization and experimental verification of coplanar interdigital electroadhesives," *Journal of Physics D: Applied Physics*, vol. 49, no. 41, p. 415304, 2016.

[27] J. Guo, T. Bamber, T. Hovell, M. Chamberlain, L. Justham, and M. Jackson, "Geometric optimisation of electroadhesive actuators based on 3d electrostatic simulation and its experimental verification," *IFAC-PapersOnLine*, vol. 49, no. 21, pp. 309–315, 2016.

[28] J. Guo, T. Bamber, J. Petzing, L. Justham, and M. Jackson, "Experimental study of relationship between interfacial electroadhesive force and applied voltage for different substrate materials," *Applied Physics Letters*, vol. 110, no. 5, p. 051602, 2017.